Understanding the relativistic overdensity of galaxy surveys

Didam G.A. Duniya
[1] *Department of Mathematics & Applied Mathematics, University of Cape Town, Cape Town 7701, South Africa*
[2] *African Institute for Mathematical Sciences (AIMS), Cape Town 7945, South Africa*
[3] *Department of Physics & Astronomy, University of the Western Cape, Cape Town 7535, South Africa*
(Dated: March 17, 2017)

The main goal of galaxy surveys is to map the distribution of the galaxies, for the purpose of understanding the properties of this distribution and its implications for the content and evolution of the universe. However, in order to realise the potential of these surveys, we need to ensure that we are using a correct analysis: a relativistic analysis, which has been extensively studied recently. In this work, the known relativistic overdensity of galaxy surveys is re-examined. Subtle, but crucial parameters which appear to have been missed by previous works are uncovered. The possible implication of these parameters on the observed galaxy power spectrum is demonstrated, in the standard concordance model. The results show that these parameters can alter the predictions of galaxy clustering on all scales; thus, the effects of relativistic corrections (on Hubble scales).

arXiv:1606.00712v2 [astro-ph.CO] 16 Mar 2017

I. INTRODUCTION

In recent years, relativistic effects [1]–[49] have been vastly studied. A number of the studies in the literature have shown how to calculate the observed clustering overdensity of galaxies in a relativistic context, i.e. the relativistic galaxy overdensity [1–11], revealing relativistic corrections to the simple Newtonian calculation that is standard for low redshift, small area surveys. Galaxy surveys with large volume coverage—spanning scales nearly and larger than the Hubble radius, reaching high redshifts—require relativistic corrections to the observed overdensity. Basically, these corrections are owing to the large-scale effects of (i) the gravitational potential, both local at the observed galaxies and also along the line of sight, and (ii) peculiar velocities, by the apparent motion of the galaxies relative to the observer; together, these constitute the so-called "relativistic effects".

Current optical surveys only cover low redshifts and sky area with dimensions which are smaller than the Hubble radius; thus, containing negligible relativistic effects. However, upcoming surveys in the optical and the radio/infrared, will extend to high redshifts and encompass large sky area—covering distance scales equal and larger than the horizon—providing deeper and richer information on the observable universe, but most importantly, on cosmological scales at the survey redshifts. On these scales, the relativistic effects become significant. These effects can, e.g. provide a means for a sensitive probe of the nature of dark energy and modified gravity: by comparing the predictions from the relativistic corrections to the observation of the forthcoming surveys.

There are two fundamental issues underlying the relativistic analysis: Firstly, we need to correctly identify the galaxy overdensity that is observed on the past light cone; secondly, we need to account for all the distortions arising from observing on the past light cone, including redshift and volume perturbations (with all relativistic effects included) [6]. These relativistic effects appear in the power spectrum of matter in redshift space. However, all of these effects together can suitably be accounted for—simply by using the fact that the physical (observed) number of the galaxies depends on two main quantities: the survey *volume* and the apparent *flux* of the sources.

Thus in this work, we rely on the dependence of the physical galaxy number on the survey volume and the apparent flux, to re-trace the known relativistic galaxy overdensity (at first order perturbation). We recover all previously calculated terms, and yet uncover subtle, but crucial (background) parameters which are missed out by previous works. We start by re-calculating the relativistic galaxy overdensity—while revealing the new parameters—in Sec. II; we relate our results to some previous works in Sec. III. In Sec. IV we give an overview of specific (flux- and volume-limited) samples of galaxy surveys and, in Sec. V we demonstrate the possible implications of the new parameters on the large-scale prediction of galaxy clustering, via the galaxy power spectrum, in the standard concordance model. We conclude in Sec. VI. (We leave out the specifics on measuring the new parameters as a future project; here we focus on their possible cosmological implications.)

II. THE RELATIVISTIC GALAXY OVERDENSITY

In cosmological surveys, observers usually look at a certain volume $v(\mathbf{n}, z)$ of the sky through a solid angle $\Omega_{\mathbf{n}}$ in a given direction $-\mathbf{n}$, at a redshift z away. Apart from the redshift, the solid angle and the intrinsic properties of the observed sources, surveys will generically also depend on cosmic magnification via the apparent flux $F(\mathbf{n}, z)$ (or luminosity) of the observed sources [5, 6, 12]. The observed flux of a source is implicitly (de)amplified in an inhomogeneous universe. (Hereafter, we use "magnification" to mean *magnification of sources*, by the amplification of their flux and/or angular size.) Thus, the physical number N of galaxies observed in an *arbitrary* survey will depend on two main quantities, which are,

the observed volume υ, and the apparent flux F of the sources—i.e. $N(\mathbf{n},z)=N\left(\upsilon(\mathbf{n},z),F(\mathbf{n},z)\right)$.

Moreover, a generic sample of cosmic objects in the sky would inherently contain both "magnified" and "unmagnified" fractions, respectively; where the magnified fraction is proportional to the magnification bias. However, the actual measurable quantity—being the number of objects per unit solid angle per redshift—would consist of all the events together, with no distinctions between these fractions. Nevertheless, these fraction can each be isolated by observations, and measured separately, given that the unmagnified fraction is volume dependent, and the magnified fraction is flux dependent.

Thus, a given volume element $d\upsilon(\mathbf{n},z)$ and flux interval $dF(\mathbf{n},z)$, within a specified redshift range dz and solid angle interval $d\Omega_{\mathbf{n}}$, will lead to $dN(\mathbf{n},z)$ galaxies:

$$\begin{aligned} dN(\mathbf{n},z) &= \tilde{n}_{\rm g}(\mathbf{n},z)d\upsilon(\mathbf{n},z)+\tilde{n}_{_F}(\mathbf{n},z)dF(\mathbf{n},z) \\ &\equiv \tilde{\mathcal{N}}_{\rm g}(\mathbf{n},z)d\Omega_{\mathbf{n}}dz, \end{aligned} \tag{1}$$

where (henceforth, a tilde denotes *redshift space*) we note that the decomposition of the total differential dN, top line in (1), follows directly from differential calculus (given that the observed sky volume is independent of the apparent flux from a source), and

$$\tilde{n}_{\rm g}\equiv\left.\frac{\partial N}{\partial\upsilon}\right|_{_{F_*}}=\int_{F_{cut}}^{F_*}dF\,\Theta(\upsilon,F), \tag{2}$$

where $F_*=F(m_*)$ denotes a given (maximum) flux value (to be specified by the experiment) with apparent magnitude m_*; $F_{cut}=F(m_{cut})$ is the instrument threshold or cut-off flux with apparent magnitude m_{cut}, and $\Theta=\partial N/(\partial\upsilon\partial F)$ (varying with both volume and flux) implicitly measures the *flux* or *luminosity function*; with,

$$\tilde{n}_{_F}\equiv\left.\frac{\partial N}{\partial F}\right|_{\upsilon_*}=\int_{\upsilon_{min}}^{\upsilon_*}d\upsilon\,\Theta(\upsilon,F), \tag{3}$$

where $\upsilon_*=\upsilon(r_*)$ denotes a given (maximum) volume at a specified distance r_*, and υ_{min} is the initial volume at a minimum distance r_{min} (at the observer, or another arbitrary position). Note that, the (ensemble) average number of galaxies per unit volume, with flux in the infinitesimal range from F to $F+dF$, is ΘdF; similarly, $\Theta d\upsilon$ gives the average number of galaxies per unit flux, with distance (or position) within the volume element from υ to $\upsilon+d\upsilon$. Consequently, we have $\tilde{n}_{\rm g}=\tilde{n}_{\rm g}(\upsilon)$ and $\tilde{n}_{_F}=\tilde{n}_{_F}(F)$ as the *effective* (or *cumulative*): galaxy number per unit volume, and galaxy number per unit flux, respectively.[1] (We notice that the number density $\tilde{n}_{\rm g}$ is evaluated at a fixed flux F_*, whereas, the number density $\tilde{n}_{_F}$ is evaluated at a fixed volume υ_*.)

Surveys like the SDSS[2] [50] and the LCRS[3] [51, 52], among others, employ two flux cut-offs: the instrument threshold (below which no source is detected; thus, being the lower bound), and a certain maximum (beyond which no source is detected; thus, being the upper bound). Thus, only sources with apparent magnitude in a given closed interval in a certain sky volume, are measured; usually, the given volume will also be demarcated by two distance (lower and upper) limits. Note that by integrating over volume, the number density $\tilde{n}_{_F}$ is independent of distance; conversely, $\tilde{n}_{\rm g}$ depends on distance.

The quantity $\tilde{\mathcal{N}}_{\rm g}=\partial N/(\partial\Omega_{\mathbf{n}}\partial z)$, given by (1), is the observed galaxy number per unit solid angle per redshift—which is what observers measure. If the survey also pertains the apparent size $\mathcal{X}$ of the sources, then the observed flux from a source will depend on the apparent size of that source, i.e. $F(\mathbf{n},z)=F(\mathcal{X}(\mathbf{n},z))$; whence,

$$\tilde{\mathcal{N}}_{\rm g}(\mathbf{n},z)=\tilde{n}_{\rm g}(\mathbf{n},z)\tilde{\mathcal{V}}(\mathbf{n},z)+\tilde{n}_{_F}(\mathbf{n},z)\tilde{\mathcal{F}}(\mathbf{n},z)\tilde{q}_{\mathcal{X}}(\mathbf{n},z), \tag{4}$$

where $\tilde{\mathcal{V}}=\partial\upsilon/(\partial\Omega_{\mathbf{n}}\partial z)$ is the volume per unit solid angle per redshift; with $\tilde{\mathcal{F}}=\partial F/\partial\mathcal{X}$ being the flux change per size interval $d\mathcal{X}$ (i.e. flux per unit size), and $\tilde{q}_{\mathcal{X}}=\partial\mathcal{X}/(\partial\Omega_{\mathbf{n}}\partial z)$ is the source size per unit solid angle per redshift. The redshift distribution of the galaxies is obtained by averaging over all solid angles: $d\bar{N}(\bar{z})=\langle\tilde{\mathcal{N}}_{\rm g}\rangle(\bar{z})dz$. Therefore, the (observed) relativistic galaxy overdensity, is obtained by

$$\begin{aligned} \Delta_{\rm g}^{\rm obs}(\mathbf{n},z) &\equiv \frac{\tilde{\mathcal{N}}_{\rm g}(\mathbf{n},z)-\langle\tilde{\mathcal{N}}_{\rm g}\rangle(\bar{z})}{\langle\tilde{\mathcal{N}}_{\rm g}\rangle(\bar{z})}, &(5)\\ &= e_{\mathcal{V}}(\bar{z})\left(\tilde{\delta}_{\rm g}(\mathbf{n},z)+\tilde{\delta}_{\mathcal{V}}(\mathbf{n},z)\right) \\ &+ e_{\mathcal{F}}(\bar{z})\,\mathcal{Q}(\bar{z})\tilde{\delta}_{\mathcal{M}}(\mathbf{n},z), &(6)\end{aligned}$$

where $\langle\tilde{\mathcal{N}}_{\rm g}\rangle=\bar{n}_{\rm g}\bar{\mathcal{V}}+\bar{n}_{_F}\bar{\mathcal{F}}\bar{q}_{\mathcal{X}}$ is the average galaxy distribution density in redshift space (hereafter, overbars denote "background" quantities, averaged over all solid angles, and $\delta\tilde{X}=\tilde{X}-\bar{X}$ is the perturbation in the given quantity $\tilde{X}$, with $|\delta\tilde{X}|\ll1$); $\tilde{\delta}_{\rm g}\equiv\delta\tilde{n}_{\rm g}/\bar{n}_{\rm g}$ is the number density contrast, and $\tilde{\delta}_{_{\mathcal{V}}}\equiv\delta\tilde{\mathcal{V}}/\bar{\mathcal{V}}$ is the volume density contrast. Moreover, by using that for magnified sources the flux per unit source size—in the background—is proportional to the underlying magnification per unit source size, i.e. $\bar{\mathcal{F}}\propto\bar{\mathcal{M}}$, we have $\partial\ln\bar{\mathcal{F}}=\partial\ln\bar{\mathcal{M}}$; consequently, $\tilde{\delta}_{\mathcal{M}}\equiv\delta\tilde{\mathcal{M}}/\bar{\mathcal{M}}=\delta\tilde{\mathcal{F}}/\bar{\mathcal{F}}$ is the magnification contrast.

The parameters $e_{\mathcal{V}}\equiv\bar{n}_{\rm g}\bar{\mathcal{V}}/\langle\tilde{\mathcal{N}}_{\rm g}\rangle$ and $e_{\mathcal{F}}\equiv\bar{n}_{_F}\bar{\mathcal{F}}\bar{q}_{\mathcal{X}}/\langle\tilde{\mathcal{N}}_{\rm g}\rangle$ are the fractional contributions by the change in volume and the change in flux, respectively, in the background sample—i.e. if the survey volume and the apparent flux

[1] Physically, it implies that $\tilde{n}_{\rm g}(\mathbf{n},z)=\tilde{n}_{\rm g}(\mathbf{n},z\,|\,F_*)$—evaluated at a fixed flux F_*—gives the cumulative number of galaxies per unit volume, with flux within the finite range $F_{cut}<F\leq F_*$, and $\tilde{n}_{_F}(\mathbf{n},z)=\tilde{n}_{_F}(\mathbf{n},z\,|\,\upsilon_*)$—evaluated at a fixed volume υ_*—gives the cumulative number of galaxies per unit flux in a given finite volume $\upsilon_{min}<\upsilon\leq\upsilon_*$ (or with distance within $r_{min}<r\leq r_*$).

[2] `http://www.sdss.org/surveys/`

[3] `http://qold.astro.utoronto.ca/~lin/lcrs.html`

are variable, then the change in volume will contribute a certain fraction $e_{\mathcal{V}}$ in the average distribution density $\langle\tilde{\mathcal{N}}_{\rm g}\rangle$, and similarly, the change in flux will also contribute a fraction $e_{\mathcal{F}}$—which together yield the identity

$$e_{\mathcal{V}}(\bar{z}) + e_{\mathcal{F}}(\bar{z}) = 1, \tag{7}$$

where for fixed-volume surveys (at fixed z) $\bar{\mathcal{V}} = 0 = e_{\mathcal{V}}$, and the entire background sample is generated by the variation in flux, with $e_{\mathcal{F}} = 1 = \bar{n}_{_F}\bar{\mathcal{F}}\bar{q}_{\mathcal{X}}/\langle\tilde{\mathcal{N}}_{\rm g}\rangle$; of which sample is ideal for pure magnification analysis, see e.g. [12]. (Fixing the apparent flux—and/or size—leads to $\bar{\mathcal{F}}\bar{q}_{\mathcal{X}} = 0 = e_{\mathcal{F}}$ with $e_{\mathcal{V}} = 1 = \bar{n}_{\rm g}\bar{\mathcal{V}}/\langle\tilde{\mathcal{N}}_{\rm g}\rangle$; thus, corresponding to a pure number-count analysis, see e.g. [3, 8, 11].) These parameters, $e_{\mathcal{V}}$ and $e_{\mathcal{F}}$, have never previously been taken into account (in the literature) in the calculation of the relativistic galaxy overdensity $\Delta_{\rm g}^{\rm obs}$.

The parameter $\mathcal{Q}$, is the cosmic *magnification bias* [5, 6, 12, 53–58], given by

$$\mathcal{Q} \equiv \left.\frac{\partial \ln \bar{\mathcal{N}}_{_F}}{\partial \ln \bar{\mathcal{F}}}\right|_{\bar{z}} = \frac{1}{2}\left(2 + 2\beta_{\mathcal{X}} - 5\beta_{_F}\right), \tag{8}$$

where we denote $\bar{\mathcal{N}}_{_F} = \bar{n}_{_F}\bar{\mathcal{F}}\bar{q}_{\mathcal{X}}$, and $\beta_{\mathcal{X}} \equiv \partial \ln \bar{q}_{\mathcal{X}}/\partial \ln \bar{\mathcal{F}}$ corresponds to a *size bias* [54–56]; with the parameter $\beta_{_F} \equiv -(2/5)\partial \ln \bar{n}_{_F}/\partial \ln \bar{\mathcal{F}} = \partial \log_{10} \bar{n}_{_F}/\partial \bar{m}$ corresponding to a *flux* or *luminosity bias* [52], and m is the apparent magnitude. Moreover, we have $\tilde{n}_{\rm g}\tilde{\mathcal{V}} = \tilde{n}_{\rm g}(\upsilon)\tilde{\mathcal{V}}(\upsilon)$ and $\tilde{\mathcal{N}}_{_F} = \tilde{\mathcal{N}}_{_F}(F)$, which implies that the relativistic *number-count overdensity* $\Delta_n^{\rm obs} \equiv \tilde{\delta}_{\rm g} + \tilde{\delta}_{\mathcal{V}}$ and the relativistic *magnification overdensity* $\Delta_{\mathcal{M}}^{\rm obs} \equiv \mathcal{Q}\tilde{\delta}_{_{\mathcal{M}}}$—which are, separately, observable—are volume υ and flux F dependent, respectively. (The methods given by e.g. [12, 54, 59, 60] can be applied to measure $\Delta_{\mathcal{M}}^{\rm obs}$.) Thus, $\Delta_{\mathcal{M}}^{\rm obs}$ and $\Delta_n^{\rm obs}$ are basically the magnified and the unmagnified parts, respectively, of the relativistic (galaxy) overdensity (6).

Moreover, for a given source, the surface brightness $\mathcal{S} \propto (F/\mathcal{X}^2)$ is a constant—and is unaffected by cosmic amplification (or magnification) of the source [54]. This implies that $\bar{F}/\bar{\mathcal{X}}^2 = $ constant, hence $\bar{\mathcal{F}} \propto \bar{\mathcal{X}}$ and we get $\beta_{\mathcal{X}} = \partial \ln \bar{q}_{\mathcal{X}}/\partial \ln \bar{\mathcal{X}}$. However, note that if the survey does not pertain the apparent size of the source, i.e. $F(\mathbf{n}, z) \neq F(\mathcal{X}(\mathbf{n}, z))$, we will have in (4): $\tilde{n}_{_F}\tilde{\mathcal{F}}\tilde{q}_{\mathcal{X}} \to \tilde{n}_{_F}\tilde{\mathcal{F}}$ and thus $\bar{\mathcal{N}}_{_F} = \bar{n}_{_F}\bar{\mathcal{F}}$, where $\tilde{\mathcal{F}}$ becomes the change in flux per unit solid-angle change per redshift change. Thus, $\beta_{\mathcal{X}} = 0$ and we get $2\mathcal{Q} = 2 - 5\beta_{_F}$; when $\mathcal{Q} = 1$, $\bar{n}_{_F} = $ *constant* and, we have $\bar{\mathcal{N}}_{_F}(\tilde{\mathcal{F}}/\nu) \propto \tilde{\mathcal{F}}/\nu$ and $\tilde{\mathcal{N}}_{_F}(\tilde{\mathcal{F}}) \propto \tilde{\mathcal{F}}$. (Note that, given $\bar{\mathcal{F}} \propto \bar{\mathcal{M}}$ we get $\bar{\mathcal{F}} = \tilde{\mathcal{F}}/\nu$, up to first order, where the factor $\nu \equiv \tilde{\mathcal{M}}/\bar{\mathcal{M}}$ quantifies the cosmic (de)magnification—see [12].)

Thus, we rewrite the relativistic overdensity (6):

$$\Delta_{\rm g}^{\rm obs}(\mathbf{n}, z) = e_{\mathcal{V}}(z)\Delta_n^{\rm obs}(\mathbf{n}, z) + e_{\mathcal{F}}(z)\Delta_{\mathcal{M}}^{\rm obs}(\mathbf{n}, z), \tag{9}$$

where the number-count overdensity $\Delta_n^{\rm obs}$ and the magnification overdensity $\Delta_{\mathcal{M}}^{\rm obs}$ are given in Appendix A. Note that the (total) relativistic overdensity $\Delta_{\rm g}^{\rm obs}$ is unique and physically defined: it does not correspond to any of the standard gauge-invariant definitions of overdensity—but it is automatically gauge-invariant [13].

III. PREVIOUS ANALYSES

It should be pointed out that previous works [3–11] have—by implication—applied the division given by (1), i.e. the division of a galaxy sample into separate "volume-dependent" and "flux-dependent" parts. The only difference is that (noting difference in notation), in the previous works, the two respective parts are first computed *individually* and later merely summed directly; however, doing so is inconsistent.

For example, in the work by Jeong et al [5] (see also [4, 6–10]), the relativistic overdensity (9) is computed in parts; firstly, the pure number-count overdensity $\tilde{\delta}_g$(no mag) is computed (see (40)–(55), by [5]), accounting for the overdensity solely owing to the change in the observed volume. Afterwards, by using that most real cosmic samples also depend on the apparent flux from the sources, the contribution solely owing to the variation in flux is then added (see (60), by [5]), given by

$$\tilde{\delta}_g = \tilde{\delta}_g(\text{no mag}) + \mathcal{Q}\delta\mathcal{M}, \tag{10}$$

i.e. given in the notation of [5], where we rightly identify $\Delta_n^{\rm obs} = \tilde{\delta}_g$(no mag) and $\Delta_{\mathcal{M}}^{\rm obs} = \mathcal{Q}\delta\mathcal{M}$; thus, (mis)leading to $e_{\mathcal{V}} = 1 = e_{\mathcal{F}}$. (It is worthy of note that, the results by Bonvin and Durrer [3] and by Challinor and Lewis [4], respectively, are both recovered by Jeong et al [5].)

However, given that the physical number of sources $N = N(\upsilon, F)$ implicitly depends on both the survey volume and the sources' apparent flux, then by differential calculus we have the total number differential dN to be fully decomposed as given by (1); thus, leading to (6) and (7). This way—i.e. the approach via (1)—we give a consistent procedure for including the *true* effect, $\mathcal{Q}\tilde{\delta}_{_{\mathcal{M}}}$, of cosmic magnification in the relativistic overdensity $\Delta_{\rm g}^{\rm obs}$.

Thus, (9) and hence, the entire analysis in Sec. II, generalize the relativistic overdensity for a *generic* survey, in which both the survey volume and the instrument flux are variable (within given intervals). Specifically, in redshift surveys (see [50–52]), as well as continuum surveys (see [22]), the instrument is fixed at a particular flux or intensity limit and, only above such limit can sources be detected. Such surveys are called, "threshold surveys," with the given limit being the instrument's "threshold."

Essentially, (9) implies that—contrary to previous analyses (see [4–10])—the volume-dependent and the flux-dependent parts, respectively, of the generic relativistic overdensity do not merely add; they are scaled down by their respective fractional contribution in the (total) redshift-space average distribution density.

IV. FLUX AND VOLUME LIMITED SAMPLES

An ideal, generic survey would involve variable volume and flux, respectively. Thus, as previously mentioned, the generated catalogue of the cosmic objects would inherently contain both "magnified" (flux-dependent)

and "unmagnified" (volume-dependent) fractions, respectively; with the observationally measurable quantity, being the number of objects per unit solid angle per redshift, consisting of all the events together (without any distinctions between these fractions). However, in practice, analyses are often done for specific samples; usually, for either flux-limited or volume-limited samples. (These sample types are discussed subsequently.) In order to construct or extract these samples, certain measurement limits are placed on the experiment.

A. The Limits

Generally, in observational cosmology, the principal limiting parameters are usually the apparent flux and the observed (geometric) cosmic depth; these invariably determine the source intrinsic brightness, i.e. luminosity. The flux is prescribed by an apparent magnitude m; the cosmic depth D is given in units of distance, and the luminosity is prescribed by an absolute magnitude M.

Basically, once limits, $m_{\rm lim}$ and $D_{\rm lim}$, are placed on the apparent magnitude and the cosmic depth, respectively, the limit on the absolute magnitude is automatically determined (via the magnitude-distance relation), by

$$M_{\rm lim} = m_{\rm lim} - 25 - 5\log_{10}(D_{\rm lim}), \tag{11}$$

where, in general, $m_{\rm lim}$ *needs not be* the apparent magnitude m_{cut} of the threshold flux (it may be any fixed value $m_{\rm lim} \leq m_{cut}$, depending on interest or the choice of investigation); usually, $D_{\rm lim} = D_L(z_{\rm lim})$ is the luminosity distance (measured in Mpc) at a given maximum redshift $z_{\rm lim}$. Note that, in reality, $M_{\rm lim}$ may be affected by the well-known K-correction, galactic extinction, and other notable effects—especially if $D_{\rm lim}$ is large, i.e. at a high redshift—thus, a more general expression for $M_{\rm lim}$ will need to incorporate these effects [61].

B. Flux-limited Samples

In flux-limited samples, the measuring instrument is operated on a fixed flux value—serving as the instrument's threshold—and only sources with flux strictly above this threshold are extracted or detected. The flux limit is fixed by the apparent magnitude limit $m_{\rm lim}$, and any source which is intrinsically brighter than the absolute limit (11), i.e. any $M < M_{\rm lim} < 0$, is extracted:

$$M = m_{\rm lim} - 25 - 5\log_{10}(r), \tag{12}$$

where we notice that the absolute magnitude $M = M(r)$ is mainly a function of the (radial) distance r only; the various sources are accessed by varying the observed distance. However, the distance is in turn, a function $r = r(z)$ of redshift z, so that computing r first requires knowing the actual redshift. Therefore, the experiment needs to have the sufficient resolution and sensitivity to determine z. This way, the individual sources are differentiated, and their actual number is counted. (The instrument picks out the individual sources.) Thus the given survey is automatically a "number-count" survey. Invariably, the survey is also a "redshift" survey, with a catalogue consisting of sky positions and luminosities of the sources. For the this type of catalogue, in particular, usually we have $m_{\rm lim} = m_{cut}$; with the source sample also termed, a "magnitude-limited" sample.

Note that, by having a flux threshold, it implies that sources at higher redshifts must have higher luminosities in order to be detected by the instrument, i.e. sources at larger r must have lower M. (Otherwise, they lead to a flux which is lower than the given instrument threshold, and are therefore filtered out.) In fact, once the magnitude limit is applied, the flux becomes irrelevant; the instrument no longer measures the variation in flux—it only registers the number of the individual sources which have flux above the (instrument) threshold. Thus, the *change in flux per unit solid-angle change per redshift change, is zero* (i.e. $\mathcal{F}q_{\mathcal{X}} = 0$); which leads to $e_{\mathcal{F}} = 0$ and, given (7), we have $e_{\mathcal{V}} = 1$. Then by (9), the given distribution is adequately described by $\Delta_n^{\rm obs}$ (appropriate for *pure* number-count analysis only, see e.g. [3, 8, 11]).

Moreover, it should be noted that in order to extract or screen for the required sources, the instrument is fixed at the limit $m_{\rm lim}$; however, in order to determine the number (density) of these sources, the integral in (2) must be evaluated from $m_* < m_{\rm lim}$ up to $m_{\rm lim}$ (noting that a lower apparent magnitude corresponds to a higher flux). Consequently, the resulting distribution (density) depends on the sources' distance, and hence, on the sky volume $v(r)$ containing r, at redshift z. Given (12), it implies that intrinsically faint sources will not be detected by the the instrument, unless they are close enough; whereas, brighter sources are detected even at large distances away. Thus the given sample is *spatially not uniform* [61]. Besides, the sample will inherit all the factors affecting M, which are mostly redshift-dependent (see the discussion below (11), on $M_{\rm lim}$).

C. Volume-limited Samples

An ideal volume-limited survey would be one done by observing a *fixed patch* of the sky at a given z, over a given period, and the flux and/or size distribution on the given sky patch is mapped. Thus, at the given redshift, the *change in volume per unit change in solid angle per change in redshift, is zero* (i.e. $\mathcal{V} = 0$); consequently, $e_{\mathcal{V}} = 0$ and $e_{\mathcal{F}} = 1$. (Such a survey would be appropriate for *pure* magnification analysis.) Similarly, given (9), the generated sample is adequately described by $\Delta_{\mathcal{M}}^{\rm obs}$.

However, volume-limited samples may also be extracted from flux-limited samples. This is usually done by (pre)specifying a maximum value $D_{\rm lim}$—at a fixed redshift $z_{\rm lim}$—for the depth of the cosmic volume to be investigated and, similarly, picking out only sources that

are intrinsically brighter than $M_{\rm lim}<0$; with luminosities specified by an absolute magnitude:

$$M = m - 25 - 5\log_{10}(D_{\rm lim}), \tag{13}$$

where we note that the absolute magnitude $M=M(m)$ is mainly a function of the apparent magnitude m only, and hence, the flux (density). Here, the sources are accessed by varying the apparent magnitude, and the sources in the extracted sample will be contained in a fixed volume $v_{\rm lim}=v(D_{\rm lim})$. Obviously, the cosmic depth $D_{\rm lim}$, which only needs to be less or equal to r_* (see Sec. II), is essentially the limiting radius of the sample—where the given sources are at particular distances $r\leq D_{\rm lim}$.

We notice that, given (13), in volume-limited samples the flux limit is no longer present and all *possible* fluxes are mapped (within the specified cosmic volume). Moreover, the extracted sample is *spatially uniform*, in the sense that the gradient of the number density vanishes, since the number density of the given sample does not vary with distance [61]. (Note that, by (13), the given source distribution depends only on the flux; the position or distance of the selected sources is irrelevant.)

V. THE OBSERVED GALAXY POWER SPECTRUM

We investigate the three-dimensional (3D) power spectrum associated with (9), with the main goal of showing how the parameters $e_{\mathcal{V}}$ and $e_{\mathcal{F}}$ affect the predictions of the large scale structure—without using any approximations, e.g. the distant-source approximation ($1/r\approx 0$), or the Limber's approxiamtion [62].

We adopt the zero anisotropic stress metric, given by

$$ds^2 = a^2\left[-(1+2\Phi)d\eta^2 + (1-2\Phi)d\mathbf{x}^2\right], \tag{14}$$

i.e. with $\Psi=\Phi$. On very large (linear) scales, the matter and the galaxy rest frames coincide (given the homogeneity and isotropy of these scales), and we can set the matter and the galaxy velocities to be equal: $V_m^{\parallel}=V_{\parallel}=V_{\rm g}^{\parallel}$, i.e. galaxies follow trajectories that are parallel to that of the underlying matter (equivalently, the galaxies are comoving with the underlying matter); hence there is essentially no momentum (ex)change between the two frames to cause any bias between the velocities [6]. However, on small (non-linear) scales, the implicit assumption of the matter-galaxy velocity equality may fail; implying velocity biasing, which may need to be taken into account.

Given (9), the observed 3D galaxy power spectrum is

$$\begin{aligned} P_{\rm g}^{\rm obs}(k,\mu,z) \;=\; & e_{\mathcal{V}}(z)^2 P_n^{\rm obs}(k,\mu,z) \\ & + 2e_{\mathcal{V}}(z)\left[1-e_{\mathcal{V}}(z)\right] P_{n\mathcal{M}}^{\rm obs}(k,\mu,z) \\ & + \left[1-e_{\mathcal{V}}(z)\right]^2 P_{\mathcal{M}}^{\rm obs}(k,\mu,z), \end{aligned} \tag{15}$$

where we used (7), with $P_n^{\rm obs}$ and $P_{\mathcal{M}}^{\rm obs}$ being the number-count and the magnification power spectra, respectively

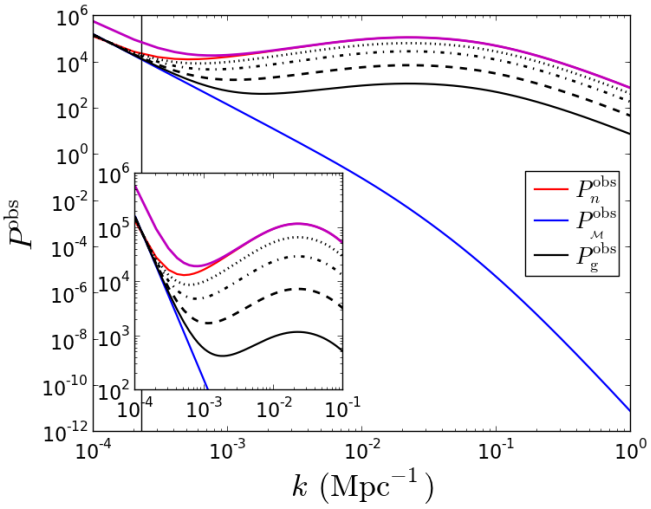

Figure 1: The plots of the radial (i.e. with $\mu=1$) linear power spectra at $z_{_S}=0.1$, with galaxy bias $b=1$ and magnification bias $\mathcal{Q}=1$. The number-count power spectrum $P_n^{\rm obs}$ (red line) has much higher power relative to the magnification power spectrum $P_{\mathcal{M}}^{\rm obs}$ (blue line)—on sub-horizon scales. The *black lines* show the full observed power spectrum $P_{\rm g}^{\rm obs}$, for the chosen parameters: $e_{\mathcal{V}}=0.1$, $e_{\mathcal{F}}=0.9$ (solid); $e_{\mathcal{V}}=0.25$, $e_{\mathcal{F}}=0.75$ (dashed); $e_{\mathcal{V}}=0.5=e_{\mathcal{F}}$ (dot-dashed), and $e_{\mathcal{V}}=0.75$, $e_{\mathcal{F}}=0.25$ (dotted). The *magenta line* shows the full observed power spectrum $\tilde{P}_{\rm g}^{\rm obs}$ with $e_{\mathcal{V}}=1=e_{\mathcal{F}}$, i.e. which corresponds to previous works in the literature. The black vertical line shows the Hubble scale.

(see Appendix B); the cross power spectrum between $\Delta_n^{\rm obs}$ and $\Delta_{\mathcal{M}}^{\rm obs}$, is given by

$$P_{n\mathcal{M}}^{\rm obs} = 2\mathcal{Q}\left[\left(b+f\mu^2+\frac{\mathcal{A}}{x^2}+\frac{\mathcal{B}}{x}\right)\mathcal{D}+\mu^2\mathcal{E}\frac{\mathcal{C}}{x}\right]P_{m\Phi}, \tag{16}$$

where the parameters in the square brackets are given in Appendices A and B, accordingly; with $P_{m\Phi}(k,z)$ being the cross power spectrum (not shown) between the matter comoving overdensity $\Delta_m(k,z)$ and the gravitational potential $\Phi(k,z)$.

To probe the galaxy power spectrum, we assume the standard late-time ΛCDM universe: dominated by a cosmological constant Λ and cold dark matter (CDM); considering mainly the very large (linear) scales. We use the present-epoch matter density parameter $\Omega_{m0}=0.24$, and the Hubble constant $H_0=73$ km $\cdot$ s^{-1} $\cdot$ Mpc^{-1}, for all numerical computations. Furthermore, we adopt a galaxy bias $b=1$, which by (A14), the evolution bias $b_e=0$. (Note that throughout this work, for simplicity, $e_{\mathcal{V}}$ and $e_{\mathcal{F}}$ are assumed to be constants; however, a proper modelling of these parameters—as functions of z—may be crucial for proper observational analysis.)

In Fig. 1, we show the plots of the radial linear power spectra (i.e. with $\mu=1$) given by (15), (B2) and (B7), respectively—at the source redshift $z_{_S}=0.1$, with magnification bias $\mathcal{Q}=1$. We see that $P_{\rm g}^{\rm obs}$ is bounded by

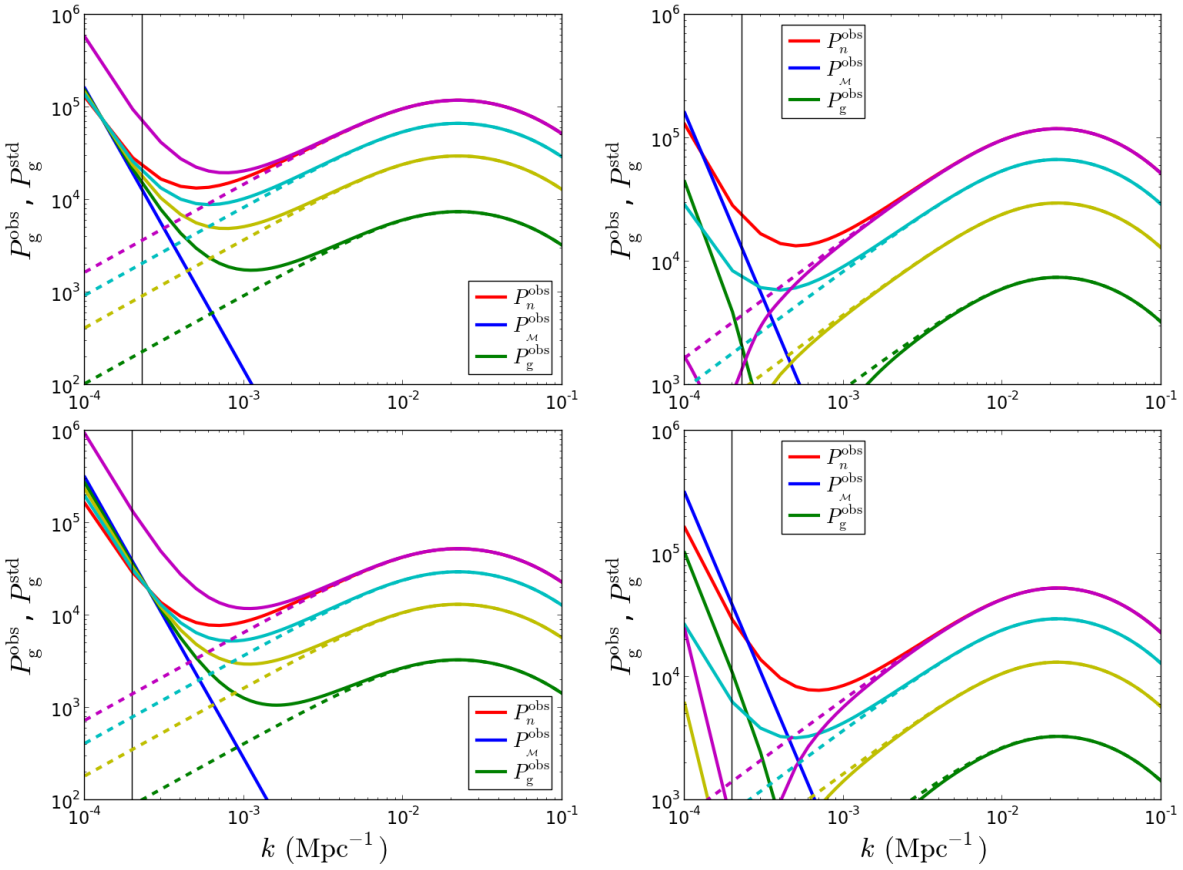

Figure 2: The plots of the radial (i.e. with $\mu = 1$) linear power spectra at $z_{\rm S} = 0.1$ (top panels) and $z_{\rm S} = 1$ (bottom panels), with galaxy bias $b = 1$; magnification bias $\mathcal{Q} = 1$ (left panels) and $\mathcal{Q} = -1$ (right panels). The number-count power spectrum $P_n^{\rm obs}$ (red line) and the magnification power spectrum $P_{\mathcal{M}}^{\rm obs}$ (blue line) are shown. The *magenta lines* show the power spectra $\tilde{P}_{\rm g}^{\rm obs}$ (solid) and $\tilde{P}_{\rm g}^{\rm std}$ (dashed) with $e_{\mathcal{V}} = 1 = e_{\mathcal{F}}$, which correspond to the analysis in previous works; the others: *solid lines* denote the full observed power spectrum $P_{\rm g}^{\rm obs}$, and *dashed lines* denote the standard power spectrum $P_{\rm g}^{\rm std}$ (see Appendix C): $e_{\mathcal{V}} = 0.25$, $e_{\mathcal{F}} = 0.75$ (green); $e_{\mathcal{V}} = 0.5 = e_{\mathcal{F}}$ (yellow), and $e_{\mathcal{V}} = 0.75$, $e_{\mathcal{F}} = 0.25$ (cyan). Vertical line shows the Hubble scale.

$P_{\mathcal{M}}^{\rm obs} \leq P_{\rm g}^{\rm obs} \leq P_n^{\rm obs}$ on all scales, as prescribed by the parameters (7): $0 \leq e_{\mathcal{V}} \leq 1$ and $e_{\mathcal{F}} = 1 - e_{\mathcal{V}}$. (The transverse power spectra, i.e. with $\mu = 0$, follow the same behaviour except that they are relatively lower in power; thus we do not show those.) Obviously, we see the effect of $e_{\mathcal{V}}$ and $e_{\mathcal{F}}$, they regulate the amplitude of $P_{\rm g}^{\rm obs}$ on all scales, by dictating the relative contributions by $P_n^{\rm obs}$ and $P_{\mathcal{M}}^{\rm obs}$, respectively. Moreover, the plots reveal that $P_n^{\rm obs}$ mostly dominates over $P_{\mathcal{M}}^{\rm obs}$ (which falls sharply towards smaller scales, i.e. increasing k). We also plot the total power spectrum $\tilde{P}_{\rm g}^{\rm obs}$, with $e_{\mathcal{V}} = 1 = e_{\mathcal{F}}$, which corresponds to the analysis by previous works in the literature. On horizon scales, we see that $\tilde{P}_{\rm g}^{\rm obs} > P_{\rm g}^{\rm obs}$ for all values of $e_{\mathcal{V}}$ and $e_{\mathcal{F}}$ obeying (7). This suggests that the relativistic effects, although already known to be small at low redshifts, may actually be lower than previously predicted—for a small magnification bias $\mathcal{Q} \ll 10$.

In Fig. 2, we show the plots of the radial power spectra, at $z_{\rm S} = 0.1$ (top panels) and at $z_{\rm S} = 1$ (bottom panels); for magnification biases $\mathcal{Q} = 1$ (left panels) and $\mathcal{Q} = -1$ (right panels), respectively. The number-count power spectrum $P_n^{\rm obs}$ and the magnification power spectrum $P_{\mathcal{M}}^{\rm obs}$ are shown, accordingly. We also show the total observed power spectrum $P_{\rm g}^{\rm obs}$, and the associated *standard* power spectrum $P_{\rm g}^{\rm std}$ (see Appendix C)—which is the power spectrum of the sum of the comoving galaxy overdensity, the redshift distortion and the net weak lensing magnification. Furthermore, the total power spectrum $\tilde{P}_{\rm g}^{\rm obs}$ and the standard power spectrum $\tilde{P}_{\rm g}^{\rm std}$ for the case where $e_{\mathcal{V}} = 1 = e_{\mathcal{F}}$ (i.e. as in previous works), are also shown. We see that, well within sub-horizon scales, $P_{\mathcal{M}}^{\rm obs} \leq P_{\rm g}^{\rm obs} \leq P_n^{\rm obs}$ for both values of $\mathcal{Q}$: at both $z_{\rm S} = 0.1$ and $z_{\rm S} = 1$. In essence, for small $\mathcal{Q} > 0$, we have $\tilde{P}_{\rm g}^{\rm obs} > P_{\rm g}^{\rm obs}$ for all scales and redshifts. In other words, if $0 \leq e_{\mathcal{V}} \leq 1$ and $e_{\mathcal{F}} = 1 - e_{\mathcal{V}}$ are not taken into account, it could lead to an incorrect prediction of the large-scale clustering of galaxies; particularly, it could lead to a false boost of the horizon-scale power—and hence, an overestimation of relativistic effects—in the observed galaxy power spectrum. However, for increasing

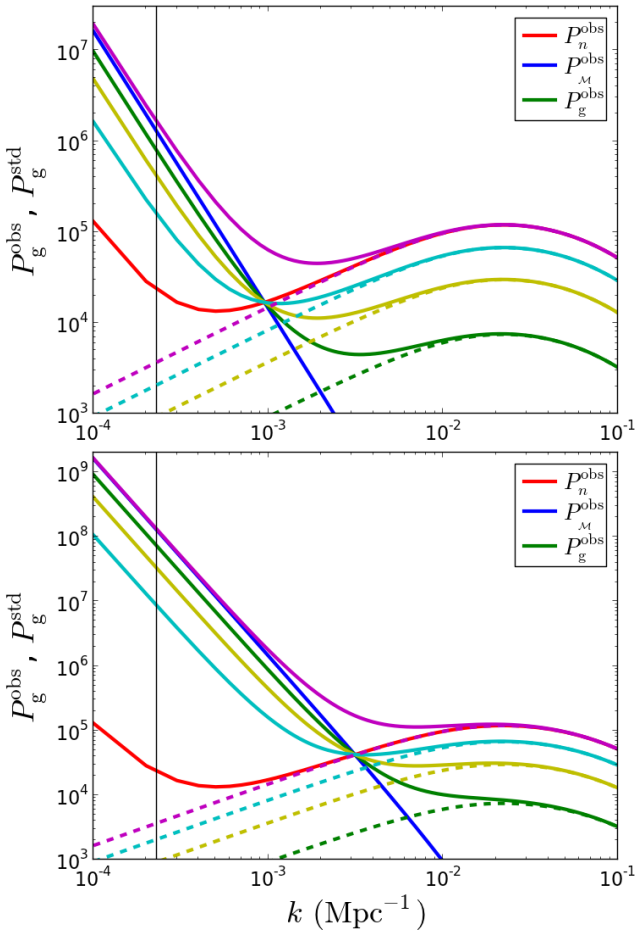

Figure 3: The plots of the radial linear power spectra at $z_{_S}=0.1$, and galaxy bias $b=1$; with magnification bias $\mathcal{Q}=10$ (top panel) and $\mathcal{Q}=100$ (bottom panel). Line notations are as in Fig. 2.

redshift (i.e. from top to bottom panels), we see a gradual growth in power (for a fixed $\mathcal{Q}$) on horizon scales, indicating large-scale growth in relativistic effects with increasing z. Moreover, at $z\gtrsim 1$, $P_{\mathcal{M}}^{\rm obs}$ starts to dominate over $P_n^{\rm obs}$ on super-horizon scales. Thus the magnification effect increases with increasing redshift. For small $\mathcal{Q}<0$, we have the reverse of the scenarios for $\mathcal{Q}>0$; while the behaviours of $P_{\rm g}^{\rm std}$ and $\tilde{P}_{\rm g}^{\rm std}$ remain unchanged throughout (they remain linear on horizon scales).

In Fig. 3 we show (for completeness) plots of the power spectra for very large $\mathcal{Q}>0$. The plots show that, increasing the value of $\mathcal{Q}\gg 1$ only results in enhancing the large-scale amplitude of the magnification power spectrum, with $|P_{\mathcal{M}}^{\rm obs}| \gg |P_n^{\rm obs}|$ on Hubble scales; consequently, for any values of $0\leq e_{_\mathcal{V}}\leq 1$ and $e_{_\mathcal{F}}=1-e_{_\mathcal{V}}$ we get $|P_{\rm g}^{\rm obs}| \leq |\tilde{P}_{\rm g}^{\rm obs}|$ (with the highest horizon-scale value of $|P_{\rm g}^{\rm obs}|$ occurring for $e_{_\mathcal{V}}\ll 1$). By comparing Figs. 2 and 3, it implies that for small magnification bias ($\mathcal{Q}\ll 10$) the relativistic effects, on super-horizon scales, are lower than previously predicted (by the analysis of previous works). Moreover, a value of e.g. $e_{_\mathcal{F}}=0.25$, implies that 25% of the observed sample occur mainly owing to the magnification of the flux (and/or angular size) of faint background sources; with the remaining 75% ($e_{_\mathcal{V}}=0.75$) occurring solely as a result of the variation, and/or distortion, in the survey volume. Basically, 25% of the observed sources have been magnified into the sample, and have a number density which varies only with flux; the remaining 75% of the sources are intrinsically bright enough to be detected, as the survey volume is varied (and these sources have a number density which depends only on volume or distance).

Moreover, notice that throughout this work we used $\mathcal{Q}(z)=constant$, which is reasonable for linear, Gaussian perturbations. However, taking non-Gaussianity [15, 17, 22, 34, 36, 39, 44] into account may lead to the transformation $\mathcal{Q}(z)\to\mathcal{Q}(z)+\Delta\mathcal{Q}(k,z)$ (via the relativistic magnification contrast $\tilde{\delta}_{_\mathcal{M}}$), where $\Delta\mathcal{Q}$ contains the non-Gaussianity (and scale) dependence; thus, changing the shape of $P_{\mathcal{M}}^{\rm obs}$ with respect to spatial scales k.

In general, the analysis in this work corresponds to an arbitrary survey. However, in practice, analyses are often done for specific samples: flux-limited, or volume-limited. Thus, care must be taken to use the appropriate relativistic overdensity, in the large-scale analysis.

VI. CONCLUSION

A clear, straightforward reanalysis of the (observed) relativistic overdensity of cosmological surveys has been given. The calculation was based on the simple fact that the physical number of sources depends mainly on the survey volume and the (source) apparent flux; consequently, giving a consistent approach for incorporating the effect of the cosmic magnification of sources, in the relativistic galaxy overdensity. Along with already known terms, new background parameters have been uncovered, and the possible consequence of these parameters in the observed galaxy power spectrum was demonstrated—in the standard, ΛCDM universe.

The new parameters separately quantify, (i) the fraction $e_{_\mathcal{F}}$ of apparently faint background sources, which have been magnified into the observed sample (by the amplification of their flux and/or angular size), and (ii) the fraction $e_{_\mathcal{V}}$ of the background sources which are apparently bright enough to be observed. These parameters dictate the contributions from the magnified (flux-dependent) and the unmagnified (volume-dependent) parts, respectively, of the relativistic overdensity; thereby regulating the amplitude of the observed (total) power spectrum. Evidently, contrary to previous analyses, the magnified and the unmagnified parts of the relativistic overdensity, in a generic survey, do not merely add; they are scaled down by $e_{_\mathcal{F}}$ and by $e_{_\mathcal{V}}$, respectively.

For small positive magnification bias $\mathcal{Q}\ll 10$, the magnification effect remains mostly sub-dominant at low redshifts $z<1$; however, this effect gradually becomes domi-

nant on horizon scales, at high redshifts $z \gtrsim 1$. Moreover, for small positive magnification bias, the relativistic effects on horizon scales may be lower than previously predicted (in the literature) in the observed power spectrum. In other words, if these new parameters are not taken into account—i.e. if they are each set to unity, $e_{\mathcal{V}} = 1 = e_{\mathcal{F}}$—this could lead to a false boost of the horizon-scale power, and hence an overestimation of the relativistic effects, in the observed galaxy power spectrum. Nevertheless, the results showed a gradual growth of the relativistic effects on horizon scales, for increasing redshift (as already known); the magnification effect also becoming prominent at higher z. (A negative magnification bias gives mostly the reverse of the scenario for a positive bias.)

In general, for a generic survey, the parameters $e_{\mathcal{V}}$ and $e_{\mathcal{F}}$ can alter the predictions of galaxy clustering on all scales, and consequently, the effect of the relativistic corrections on horizon scales. However, care must be taken to use the relativistic overdensity appropriately, e.g. when considering pure number-count surveys ($e_{\mathcal{V}} = 1$, $e_{\mathcal{F}} = 0$) or pure magnification surveys ($e_{\mathcal{V}} = 0$, $e_{\mathcal{F}} = 1$). The proper underlying conditions and/or regimes of approximation need to be observed.

Acknowledgements: Thanks to Roy Maartens and Chris Clarkson for meaningful discussions, and Daniele Bertacca for useful comments. This work was carried out with financial support from (i) the government of Canada's International Development Research Centre (IDRC), and within the framework of the AIMS Research for Africa Project, and (ii) the South African Square Kilometre Array Project and the South African National Research Foundation.

Appendix A: The Number-count and the Magnification Overdensities

In this section we give the explicit forms of the perturbation terms in (6), i.e. the density distortion $\tilde{\delta}_{\rm g}$, the volume distortion $\tilde{\delta}_{\mathcal{V}}$ and the magnification distortion $\tilde{\delta}_{\mathcal{M}}$. (Throughout this work, flat space is assumed—with most of the calculations being drawn from the rigorous work by [6, 12], and relevant references therein.)

1. The metric

We adopt a general metric, given by

$$\begin{aligned} ds^2 &= a(\eta)^2\Big\{ -(1+2\phi)\, d\eta^2 + 2B_{|i}\, d\eta dx^i \\ &\quad + \left[(1-2\psi)\delta_{ij} + 2E_{|ij}\right] dx^i dx^j \Big\}, \end{aligned} \tag{A1}$$

where a is the scale factor, and η is the conformal time; $\psi \equiv D + \frac{1}{3}\nabla^2 E$, and we have used

$$\bar{g}_{00} = -1, \quad \bar{g}_{i0} = \vec{0} = \bar{g}_{0j}, \quad \bar{g}_{ij} = \delta_{ij}, \tag{A2}$$

and given the 4-scalars $\phi = \phi(\eta, x^i)$, $B = B(\eta, x^i)$, $D = D(\eta, x^i)$ and $E = E(\eta, x^i)$:

$$\delta g_{00} = -2\phi, \quad \delta g_{i0} = B_i, \quad \delta g_{ij} = -2\left(D\delta_{ij} - E_{ij}\right), \tag{A3}$$

where $B_i = B_{|i}$ and $E_{ij} = E_{|ij} - \frac{1}{3}\delta_{ij}\nabla^2 E$ is a traceless transverse tensor—i.e. $E^i{}_i = 0$, such that it has no contribution to the term, $D\delta^i{}_i$, in the diagonal plane. (Note that, $X_{|i} \equiv \nabla_i X$, and $X_{|ij} \equiv \nabla_i \nabla_j X$ for a scalar X.)

The 4-velocities of a particle moving in ds, are

$$\begin{aligned} u^\mu &= a^{-1}\left(1-\phi,\ v_{|i}\right), \\ u_\mu &= a\left(-1-\phi,\ v_{|i} + B_{|i}\right), \end{aligned} \tag{A4}$$

where v is the velocity potential (a scalar).

Given (A1)–(A4), we define the following potentials

$$\Phi \equiv \phi - \mathcal{H}\sigma - \sigma', \tag{A5}$$

$$\Psi \equiv D + \frac{1}{3}\nabla^2 E + \mathcal{H}\sigma, \tag{A6}$$

$$V \equiv v + E', \tag{A7}$$

which are all gauge-invariant, where $\sigma = -B + E'$; $\mathcal{H} = a'/a$ is the comoving Hubble parameter, and a prime denotes derivative with respect to conformal time.

2. The density distortion

Here we give the expression for the distortion $\tilde{\delta}_{\rm g}$ arising in the galaxy number density $\tilde{n}_{\rm g}$. In order to compute $\tilde{\delta}_{\rm g}(\mathbf{n}, z)$, which is in redshift space, we need to relate it to the distortion $\delta_{\rm g}(\mathbf{x}, \eta)$ in real space $\mathbf{x}$. Thus by taking a gauge transformation from real to redshift space:

$$\tilde{\delta}_{\rm g}(\mathbf{n}, z) = \delta_{\rm g}(\mathbf{n}, z) - \frac{d\ln \bar{n}_{\rm g}}{d\bar{z}}\, \delta z(\mathbf{n}, z), \tag{A8}$$

where the background number density $\bar{n}_{\rm g}$ remains the same in both real and redshift spaces, respectively. We have used that, to first order, $\delta\eta = (\partial\bar{\eta}/\partial\bar{z})\delta z$. We have

$$\frac{d}{d\bar{z}} \ln \bar{n}_{\rm g}(\bar{z}) = \frac{3 - b_e(\bar{z})}{1+\bar{z}}, \tag{A9}$$

where we used $a = (1+\bar{z})^{-1}$, and the linear galaxy *evolution bias* [5, 6] is given by

$$b_e \equiv \left.\frac{\partial \ln(a^3 \bar{n}_{\rm g})}{\partial \ln(a)}\right|_{\bar{z}}, \tag{A10}$$

with $a^3\bar{n}_{\rm g}$ being the background *comoving* galaxy number per unit volume.

A photon which propagates along the direction $\mathbf{n}$ from a source S will be seen by an observer O, located elsewhere in the universe with fundamental 4-velocity u^μ, to be moving with an energy $\mathcal{E} = -n^\mu u_\mu$ under the direction $-\mathbf{n}$. The redshift z of the propagating photon, in

moving from S to O is given by (see [3, 6] for details)

$$1+z \;=\; (1+\bar{z})\Big[1+(\Phi+\Psi+\mathbf{n}\cdot\mathbf{V}-\psi)\big|_{z_S}^{0} - \int_{\bar{r}_S}^{0} d\bar{r}\,(\Phi'+\Psi')\Big], \tag{A11}$$

where $\bar{r}_{_S}=\bar{r}(\bar{z}_{_S})$ is the background comoving distance at S, ψ is a scalar metric potential, and $\mathbf{V}=\partial_i V$. The parameters Φ, Ψ and V are given by (A5)–(A7). A prime (henceforth) denotes derivative with respect to conformal time η. Hence given (A9) and (A11), the density distortion (A8) becomes

$$\begin{aligned}\tilde{\delta}_{\rm g}(\mathbf{n},z) \;&=\; \Delta_\psi(\mathbf{n},z)+3\,(\Phi+\Psi)\,(\mathbf{n},z)+3\,\mathbf{n}\cdot\mathbf{V}(\mathbf{n},z)\\ &+\; 3\int_{\bar{r}_S}^{0} d\bar{r}\,(\Phi'+\Psi')\,(\mathbf{n},z)-b_e(\bar{z})\Big[\Phi(\mathbf{n},z)\\ &+\; \mathbf{n}\cdot\mathbf{V}(\mathbf{n},z)+\int_{\bar{r}_S}^{0} d\bar{r}\,(\Phi'+\Psi')\,(\mathbf{n},z)\Big],\end{aligned} \tag{A12}$$

where $\Delta_\psi\equiv\delta_{\rm g}-3\psi-b_e\mathcal{H}\sigma$ is the overdensity in flat slicing; terms outside integrals are the relative values between S and O. (Note that the b_e term in (A12) has been missed by [3, 11].) Thus, we obtain

$$\Delta_\psi \;=\; \Delta_{\rm g}+(3-b_e)\,\mathcal{H}V-3\Psi, \tag{A13}$$

where $\Delta_{\rm g}\equiv\delta_{\rm g}+\bar{n}'_{\rm g}(v+B)/\bar{n}_{\rm g}$ is the galaxy comoving overdensity. The galaxy and the matter comoving overdensities, respectively, are related by $\Delta_{\rm g}=b\Delta_m$ (see e.g. [6] for a derivation)—where b is the linear *galaxy bias* [5, 6, 15, 16]. The (Gaussian) galaxy bias relates to the evolution bias (A10), by [6]

$$b \;=\; -\mathcal{H}\,(3-b_e)\,\frac{\bar{\rho}_m}{\bar{\rho}'_m} \;=\; 1-\frac{1}{3}b_e, \tag{A14}$$

where the second equality follows from the standard continuity equation $\bar{\rho}'_m=-3\mathcal{H}\bar{\rho}_m$.

3. The volume distortion

The distortion that arises in the observed volume of galaxy redshift surveys, i.e. the volume density contrast $\tilde{\delta}_{\mathcal{V}}$, is given by (see [3, 6, 12] for details)

$$\begin{aligned}\tilde{\delta}_{\mathcal{V}} \;&=\; -4\,\mathbf{n}\cdot\mathbf{V}+\int_0^{\bar{r}_S} d\bar{r}\,(\bar{r}-\bar{r}_{_S})\,\frac{\bar{r}}{\bar{r}_{_S}}\nabla_\perp^2\,(\Phi+\Psi)\\ &+3\int_0^{\bar{r}_S} d\bar{r}\,(\Phi'+\Psi')+\frac{2}{\bar{r}_{_S}}\int_0^{\bar{r}_S} d\bar{r}\,(\Phi+\Psi)\\ &+\left(\frac{\mathcal{H}'}{\mathcal{H}^2}+\frac{2}{\bar{r}_{_S}\mathcal{H}}\right)\left[\Phi+\mathbf{n}\cdot\mathbf{V}-\int_0^{\bar{r}_S} d\bar{r}\,(\Phi'+\Psi')\right]\\ &+\frac{1}{\mathcal{H}}\left[\Psi'+\partial_r\Phi-\frac{d}{d\lambda}\mathbf{n}\cdot\mathbf{V}\right]-2\,(\Phi+\Psi)\,,\end{aligned} \tag{A15}$$

where the squared gradient $\nabla_\perp^2=\nabla^2-\partial_r^2-2\bar{r}^{-1}\partial_r$ (with $\partial_r=-\bar{n}^i\partial_i$) is the Laplacian on the surface transverse to the line of sight, and λ is an affine parameter along the photon trajectory: $dX/d\lambda=X'-\partial_r X$ (i.e. X being a scalar). By using that galaxies (hence, pressureless matter) move along geodesics, we have the Euler equation for the line-of-sight velocity as

$$\mathbf{n}\cdot\mathbf{V}'+\mathcal{H}\mathbf{n}\cdot\mathbf{V}-\partial_r\Phi \;=\; 0. \tag{A16}$$

Thus given (A12), (A13), (A15) and (A16), the (observed) number-count overdensity is [6]

$$\begin{aligned}\Delta_n^{\rm obs}(\mathbf{n},z) \;&=\; \Delta_{\rm g}(\mathbf{n},z)-\frac{1}{\mathcal{H}}\partial_r V_\parallel(\mathbf{n},z)\\ &+\int_0^{\bar{r}_S} d\bar{r}\,(\bar{r}-\bar{r}_{_S})\,\frac{\bar{r}}{\bar{r}_{_S}}\nabla_\perp^2\,(\Phi+\Psi)\,(\mathbf{n},z)\\ &+\;(3-b_e)\,\mathcal{H}V(\mathbf{n},z)+\frac{1}{\mathcal{H}}\Psi'(\mathbf{n},z)\\ &-\;\left(b_e-1-\frac{\mathcal{H}'}{\mathcal{H}^2}-\frac{2}{\bar{r}_{_S}\mathcal{H}}\right)\Phi(\mathbf{n},z)\\ &-\;2\Psi(\mathbf{n},z)+\frac{2}{\bar{r}_{_S}}\int_0^{\bar{r}_S} d\bar{r}\,(\Phi+\Psi)\,(\mathbf{n},z)\\ &+\;\left(b_e-\frac{\mathcal{H}'}{\mathcal{H}^2}-\frac{2}{\bar{r}_{_S}\mathcal{H}}\right)\Big[V_\parallel(\mathbf{n},z)\\ &\qquad+\int_0^{\bar{r}_S} d\bar{r}\Big(\Phi'+\Psi'\Big)(\mathbf{n},z)\Big],\end{aligned} \tag{A17}$$

where $\bar{r}$, b_e and $\mathcal{H}$ are functions of $\bar{z}$; with $V_\parallel\equiv-\mathbf{n}\cdot\mathbf{V}=\partial_r V$ being the line-of-sight component of the velocity $\mathbf{V}$, as seen by O. The first two lines give the "standard" term of the relativistic number-count overdensity: consisting of the comoving galaxy overdensity, the (Kaiser) redshift distortion term and the weak (gravitational) lensing term, respectively. The standard term constitutes the most dominant contributions (especially at low z). The rest of the lines together constitute the "relativistic corrections"; with the third, fourth and fifth lines giving the (peculiar velocity and gravitational) potential effect and the time delay [31] (integral term) in the photon signals. In the last two lines, the first and the second terms in the square brackets correspond to the Doppler and the integrated Sachs-Wolfe (ISW) effects, respectively.

4. The magnification distortion

Similarly, a lengthy but straightforward calculation (see [5, 6, 12] for details) yields the magnification distortion $\tilde{\delta}_{\mathcal{M}}$; hence the (observed) relativistic magnification

overdensity becomes

$$\begin{aligned}\Delta^{\rm obs}_{\mathcal{M}}(\mathbf{n},z) &= \mathcal{Q}(\bar{z})\int_0^{\bar{r}_S} d\bar{r}\,(\bar{r}_S-\bar{r})\,\frac{\bar{r}}{\bar{r}_S}\nabla^2_\perp\,(\Phi+\Psi)\,(\mathbf{n},z)\\ &+ 2\mathcal{Q}(\bar{z})\Psi(\mathbf{n},z)-\frac{2\mathcal{Q}(\bar{z})}{\bar{r}_S}\int_0^{\bar{r}_S} d\bar{r}\,(\Phi+\Psi)\\ &+ 2\mathcal{Q}(\bar{z})\left(1-\frac{1}{\bar{r}_S\mathcal{H}}\right)\Big[\Phi(\mathbf{n},z)-V_\parallel(\mathbf{n},z)\\ &\quad-\int_0^{\bar{r}_S} d\bar{r}\,(\Phi'+\Psi')\,(\mathbf{n},z)\Big], \qquad \text{(A18)}\end{aligned}$$

where the first line gives the weak lensing term, and the remaining lines give the relativistic effects. Thus, by combining (A17) and (A18) we get the explicit form of the (observed) relativistic galaxy overdensity (9)—taking note of (7).

In general, note that the overdensity $\Delta^{\rm obs}_{\mathcal{M}}$ solely measures the "magnification of sources"—owing mainly to the magnification of the sources' fluxes by (A18): weak lensing, Doppler effect, ISW effect, time delay and (gravitational) potential difference (see [12] for concise statements on these effects, pertaining the magnification of sources). Similarly, the redshift distortions, weak lensing, Doppler effect, ISW effect, time delay and potential difference effects also combine to induce distortions $\tilde{\delta}_{\mathcal{V}}$ in the survey volume (see (A15))—which then increases (or decreases) the number of counted sources—resulting in the "(de)amplification of the number-count overdensity" $\Delta^{\rm obs}_n$. Moreover, notice that there are still some residual lensing/magnification effects left in $\Delta^{\rm obs}_n$; however, these effects are mainly owing to the inherent volume distortion $\tilde{\delta}_{\mathcal{V}}$, and not owing to dependence on flux/luminosity.

Appendix B: The Number-count and the Magnification Power Spectra

We compute the various 3D (linear) power spectra of the observed overdensities $\Delta^{\rm obs}_n$ in (A17) and $\Delta^{\rm obs}_{\mathcal{M}}$ in (A18), repectively (in Fourier space).

1. The number-count power spectrum

Consider the galaxy relativistic number-count overdensity (A17), then we can transform it in terms of the matter comoving overdensity Δ_m—given in Fourier space by

$$\Delta^{\rm obs}_n = \left[b+f\mu^2+\frac{\mathcal{A}}{x^2}+\frac{\mathcal{B}}{x}+i\mu\frac{\mathcal{C}}{x}\right]\Delta_m, \qquad \text{(B1)}$$

where $f\equiv k^2V_m/(\mathcal{H}\Delta_m)$ is a parameter which measures the (Kaiser) redshift distortions (in the concordance model, f becomes the standard matter *linear growth rate*—as shown by [6]); $\mu=-\mathbf{n}\cdot\mathbf{k}/k$, with $\mathbf{k}$ and $k=|\mathbf{k}|$ being the wave vector and the wavenumber, respectively; $x\equiv k/\mathcal{H}$ is a dimensionless parameter. Thus given (B1),

$$\begin{aligned}\frac{P^{\rm obs}_n}{P_m} &= \left(b+f\mu^2\right)^2+2\left(b+f\mu^2\right)\left[\frac{\mathcal{A}}{x^2}+\frac{\mathcal{B}}{x}\right]\\ &+\left[\frac{\mathcal{A}}{x^2}+\frac{\mathcal{B}}{x}\right]^2+\mu^2\frac{\mathcal{C}^2}{x^2}, \qquad \text{(B2)}\end{aligned}$$

where $P_m(k,z)$ is the DM linear power spectrum (see [6, 13, 38]), and

$$\mathcal{A} \equiv (3-b_e)f-x^2\left[b_e+1-\frac{\mathcal{H}'}{\mathcal{H}^2}-\frac{2}{\bar{r}_S\mathcal{H}}+\frac{\Phi'}{\mathcal{H}\Phi}\right]\frac{\Phi}{\Delta_m}, \qquad \text{(B3)}$$

$$\mathcal{B} \equiv \frac{2x}{\Delta_m}\left\{\int_0^{\bar{r}_S} d\tilde{r}\left[\frac{2}{\bar{r}_S}-(1-\mu^2)(\tilde{r}-\bar{r}_S)\frac{\tilde{r}}{\bar{r}_S}k^2\right]\tilde{\Phi}+\left(b_e-\frac{\mathcal{H}'}{\mathcal{H}^2}-\frac{2}{\bar{r}_S\mathcal{H}}\right)\int_0^{\bar{r}_S} d\tilde{r}\tilde{\Phi}'\right\}, \qquad \text{(B4)}$$

$$\mathcal{C} \equiv -\left(b_e-\frac{\mathcal{H}'}{\mathcal{H}^2}-\frac{2}{\bar{r}_S\mathcal{H}}\right)f+\frac{4x}{\bar{r}_S\Delta_m}\int_0^{\bar{r}_S} d\tilde{r}(\tilde{r}-\bar{r}_S)k\tilde{\Phi}, \qquad \text{(B5)}$$

where the variable $\tilde{\Phi}=\Phi(k,\tilde{r})$ is the invariant gravitational potential evaluated at a background comoving distance $\tilde{r}$—at an arbitrary position between S and O.

2. The magnification power spectrum

Here we consider the relativistic magnification overdensity (A18) of magnified galaxies. We transform the magnification overdensity in terms of the gauge-invariant gravitational potential:

$$\Delta^{\rm obs}_{\mathcal{M}} = 2\mathcal{Q}\left[\mathcal{D}+i\mu\mathcal{E}\right]\Phi, \qquad \text{(B6)}$$

and consequently, we obtain the associated magnification linear power spectrum—given by

$$P^{\rm obs}_{\mathcal{M}} = 4\mathcal{Q}^2\left(\mathcal{D}^2+\mu^2\mathcal{E}^2\right)P_\Phi, \qquad \text{(B7)}$$

with $P_\Phi(k,z)$ being the linear power spectrum of the gravitational potential, and

$$\mathcal{D} \equiv 2-\frac{1}{\bar{r}_S\mathcal{H}}-\frac{1}{\Phi}\Big\{2\Big(1-\frac{1}{\bar{r}_S\mathcal{H}}\Big)\int_0^{\bar{r}_S}d\tilde{r}\tilde{\Phi}' + \int_0^{\bar{r}_S}d\tilde{r}\Big[\frac{2}{\bar{r}_S}-(1-\mu^2)(\tilde{r}-\bar{r}_S)\frac{\tilde{r}}{\bar{r}_S}k^2\Big]\tilde{\Phi}\Big\}, \quad \text{(B8)}$$

$$\mathcal{E} \equiv x\Big(1-\frac{1}{\bar{r}_S\mathcal{H}}\Big)\frac{\mathcal{H}V_m}{\Phi}-\frac{2}{\bar{r}_S\Phi}\int_0^{\bar{r}_S}d\tilde{r}(\tilde{r}-\bar{r}_S)k\tilde{\Phi}, \quad \text{(B9)}$$

where we note that in (B8), similarly in (B4), the main contribution of the lensing source-term $\nabla^2_\perp\Phi$ in Fourier space only adds to the transverse power spectrum (with $\mu=0$), since the radial (line-of-sight) power spectrum (with $\mu=1$) has this term to be zero. Moreover, for the transverse power spectrum: the Kaiser redshift distortion term together with all the complex terms—i.e. the parameters $f\Delta_m$, $\mathcal{C}$ and $\mathcal{E}$—are eliminated.

Appendix C: The Standard Galaxy Power Spectrum

Given the parameters $e_\mathcal{V}$ and $e_\mathcal{F}$, here we give the "standard" overdensity—which is made up by the comoving (galaxy) overdensity, the redshift distortion and the total lensing terms—by (in real space)

$$\Delta_{\rm g}^{\rm std} \equiv (1-\mathcal{Q}_{\rm eff})\int_0^{\bar{r}_S}d\tilde{r}\,(\tilde{r}-\bar{r}_S)\,\frac{\tilde{r}}{\bar{r}_S}\nabla^2_\perp(\tilde{\Phi}+\tilde{\Psi}) + e_\mathcal{V}\Big(\Delta_{\rm g}+\frac{1}{\mathcal{H}}\partial_r V_\parallel\Big), \quad \text{(C1)}$$

where used (9), (A17) and (A18); $1-\mathcal{Q}_{\rm eff}\equiv e_\mathcal{V}-e_\mathcal{F}\mathcal{Q}$ defines an "effective" magnification bias. In Fourier space,

$$\Delta_{\rm g}^{\rm std} = \Big[e_\mathcal{V}\left(b+f\mu^2\right)+(1-\mathcal{Q}_{\rm eff})\left(\frac{\mathcal{K}}{x}+i\mu\frac{\mathcal{R}}{x}\right)\Big]\Delta_m, \quad \text{(C2)}$$

where f and μ are as given in (B1); given the metric (14),

$$\mathcal{K} \equiv -\frac{2x}{\Delta_m}\int_0^{\bar{r}_S}d\tilde{r}(1-\mu^2)\,(\tilde{r}-\bar{r}_S)\,\frac{\tilde{r}}{\bar{r}_S}k^2\tilde{\Phi}, \quad \text{(C3)}$$

$$\mathcal{R} \equiv \frac{4x}{\bar{r}_S\Delta_m}\int_0^{\bar{r}_S}d\tilde{r}\,(\tilde{r}-\bar{r}_S)\,k\tilde{\Phi}. \quad \text{(C4)}$$

Consequently, we have

$$\frac{P_{\rm g}^{\rm std}}{P_m} = e_\mathcal{V}^2\left(b+f\mu^2\right)^2+2e_\mathcal{V}\,(1-\mathcal{Q}_{\rm eff})\left(b+f\mu^2\right)\frac{\mathcal{K}}{x} + (1-\mathcal{Q}_{\rm eff})^2\frac{\mathcal{K}^2}{x^2}+(1-\mathcal{Q}_{\rm eff})^2\mu^2\frac{\mathcal{R}^2}{x^2}, \quad \text{(C5)}$$

which is the associated standard power spectrum.

[1] J. Yoo, A. L. Fitzpatrick and M. Zaldarriaga, Phys. Rev. D **80**, 083514 (2009) [arXiv:0907.0707].
[2] J. Yoo, Phys. Rev. D **82**, 083508 (2010) [arXiv:1009.3021].
[3] C. Bonvin and R. Durrer, Phys. Rev. D **84**, 063505 (2011) [arXiv:1105.5280].
[4] A. Challinor and A. Lewis, Phys. Rev. D **84**, 043516 (2011) [arXiv:1105.5292].
[5] D. Jeong, F. Schmidt and C. M. Hirata, Phys. Rev. D **85**, (2012) 023504 [arXiv:1107.5427].
[6] D. Duniya, Ph.D. thesis, University of the Western Cape, South Africa (2015).
[7] C. Bonvin, Class. Quant. Grav. **31**, 234002 (2014) [arXiv:1409.2224].
[8] L. Lopez-Honorez, O. Mena and S. Rigolin, Phys. Rev. D **85**, 023511 (2012) [arXiv:1109.5117].
[9] D. Alonso, P. Bull, P. G. Ferreira, R. Maartens and M. Santos, Astrophys. J. **814**, 145 (2015) [arXiv:1505.07596].
[10] J. Renk, M. Zumalacarregui and F. Montanari, JCAP **1607**, 040 (2016) [arXiv:1604.03487].
[11] R. Durrer and V. Tansella, JCAP **1607**, 037 (2016) [arXiv:1605.05974].
[12] D. Duniya, Phys. Rev. D **93**, 103538 (2016) [arXiv:1604.03934].
[13] D. Duniya, D. Bertacca and R. Maartens, JCAP **1310**, 015 (2013) [arXiv:1305.4509].
[14] F. Montanari and R. Durrer, JCAP **1510**, 070 (2015) [arXiv:1506.01369].
[15] N. Bartolo, S. Matarrese and A. Riotto, JCAP **1104**, 011 (2011) [arXiv:1011.4374].
[16] T. Baldauf, U. Seljak, L. Senatore and M. Zaldarriaga, JCAP **1110**, 031 (2011) [arXiv:1106.5507].
[17] J. Yoo, N. Hamaus, U. Seljak and M. Zaldarriaga, Phys. Rev. D **86**, 063514 (2012) [arXiv:1109.0998].
[18] F. Schmidt and D. Jeong, Phys. Rev. D **86**, 083527 (2012) [arXiv:1204.3625].
[19] D. Jeong and F. Schmidt, Phys. Rev. D **86**, 083512 (2012) [arXiv:1205.1512].
[20] F. Schmidt and D. Jeong, Phys. Rev. D **86**, 083513 (2012) [arXiv:1205.1514].
[21] D. Bertacca, R. Maartens, A. Raccanelli and C. Clarkson, JCAP **1210**, 025 (2012) [arXiv:1205.5221].
[22] R. Maartens, G. B. Zhao, D. Bacon, K. Koyama and A. Raccanelli, JCAP **1302**, 044 (2013) [arXiv:1206.0732].
[23] S. F. Flender and D. J. Schwarz, Phys. Rev. D **86**, 063527

(2012) [arXiv:1207.2035].
[24] A. Hall, C. Bonvin and A. Challinor, Phys. Rev. D **6**, 2013 (87) [arXiv:1212.0728].
[25] L. Lombriser, J. Yoo and K. Koyama, Phys. Rev. D **87**, 104019 (2013) [arXiv:1301.3132].
[26] J. Yoo and V. Desjacques, Phys. Rev. D **88**, 023502 (2013) [arXiv:1301.4501].
[27] D. Jeong and F. Schmidt, Phys. Rev. D **89**, 043519 (2014) [arXiv:1305.1299].
[28] A. Raccanelli, D. Bertacca, O. Dore and R. Maartens, JCAP **1408**, 022 (2014) [arXiv:1306.6646].
[29] E. Di Dio, F. Montanari, J. Lesgourgues and R. Durrer, JCAP **1311**, 044 (2013) [arXiv:1307.1459].
[30] C. Bonvin, L. Hui and E. Gaztanaga, Phys. Rev. D **89**, 083535 (2014) [arXiv:1309.1321].
[31] A. Raccanelli, D. Bertacca, R. Maartens, C. Clarkson and O. Dore, Gen. Rel. Grav. **48**, 84 (2016) [arXiv:1311.6813].
[32] D. J. Bacon, S. Andrianomena, C. Clarkson, K. Bolejko and R. Maartens, Mon. Not. Roy. Astron. Soc. **443**, 1900 (2014) [arXiv:1401.3694].
[33] D. Jeong and F. Schmidt, Class. Quant. Grav. **32**, 044001 (2015) [arXiv:1407.7979].
[34] E. Villa, L. Verde and S. Matarrese, Class. Quant. Grav. **31**, 234005 (2014) [arXiv:1409.4738].
[35] J. Yoo, Class. Quant. Grav. **31**, (2014) 234001 [arXiv:1409.3223].
[36] S. Camera, M. G. Santos and R. Maartens, Mon. Not. Roy. Astron. Soc. **448**, 1035 (2015) [arXiv:1409.8286].
[37] S. Camera, R. Maartens and M. G. Santos, Mon. Not. Roy. Astron. Soc. **451**, L80 (2015) [arXiv:1412.4781].
[38] D. Duniya, D. Bertacca and R. Maartens, Phys. Rev. D **91**, 063530 (2015) [arXiv:1502.06424].
[39] A. Kehagias, A. M. Dizgah, J. Norena, H. Perrier and A. Riotto, JCAP **1508**, 018 (2015) [arXiv:1503.04467].
[40] D. Duniya, Gen. Rel. Grav. **48**, 52 (2016) [arXiv:1505.03436].
[41] A. Raccanelli, F. Montanari, D. Bertacca, O. Dore and R. Durrer, JCAP **1605**, 009 (2016) [arXiv:1505.06179].
[42] N. Bartolo *et al.*, Phys. Dark Univ. **13**, 30 (2016) [arXiv:1506.00915].
[43] D. Alonso and P. G. Ferreira, Phys. Rev. D **92**, 063525 (2015) [arXiv:1507.03550].
[44] J. Yoo and J. O. Gong, Phys. Lett. B **754**, 94 (2016) [arXiv:1509.08466].
[45] V. Irsic, E. Di Dio and M. Viel, JCAP **1602**, 051 (2016) [arXiv:1510.03436].
[46] E. Di Dio, R. Durrer, G. Marozzi and F. Montanari, JCAP **1601**, 016 (2016) [arXiv:1510.04202].
[47] C. Bonvin, L. Hui and E. Gaztanaga, JCAP **1608**, 021 (2016) [arXiv:1512.03566].
[48] E. Gaztanaga, C. Bonvin and L. Hui, JCAP **1701**, 032 (2017) [arXiv:1512.03918].
[49] A. Raccanelli, D. Bertacca, D. Jeong, M. C. Neyrinck and A. S. Szalay, arXiv:1602.03186.
[50] F. D. Albareti *et al.* [SDSS Collaboration], arXiv:1608.02013.
[51] S. A. Shectman, S. D. Landy, A. Oemler, D. L. Tucker, H. Lin, R. P. Kirshner and P. L. Schechter, Astrophys. J. **470**, 172 (1996) [astro-ph/9604167].
[52] H. Lin, R. P. Kirshner, S. A. Shectman, S. D. Landy, A. Oemler, D. L. Tucker and P. L. Schechter, Astrophys. J. **471**, 617 (1996) [astro-ph/9606055].
[53] R. Ziour and L. Hui, Phys. Rev. D **78**, 123517 (2008) [arXiv:0809.3101].
[54] F. Schmidt, E. Rozo, S. Dodelson, L. Hui and E. Sheldon, Phys. Rev. Lett. **103**, 051301 (2009) [arXiv:0904.4702].
[55] F. Schmidt and E. Rozo, Astrophys. J. **735**, 119 (2011) [arXiv:1009.0757].
[56] J. Liu, Z. Haiman, L. Hui, J. M. Kratochvil and M. May, Phys. Rev. D **89**, 023515 (2014) [arXiv:1310.7517].
[57] S. Camera, C. Fedeli and L. Moscardini, JCAP **1403**, 027 (2014) [arXiv:1311.6383].
[58] H. Hildebrandt, Mon. Not. Roy. Astron. Soc. **455**, 3943 (2016) [arXiv:1511.01352].
[59] A. F. Heavens and B. Joachimi, Mon. Not. Roy. Astron. Soc. **415**, 1681 (2011) [arXiv:1101.3337].
[60] B. Gillis and A. Taylor, Mon. Not. Roy. Astron. Soc. **456**, 2518 (2016) [arXiv:1507.01858].
[61] V. J. Martinez and E. Saar, *Statistics of the Galaxy Distribution*, Chapman & Hall/CRC (2002).
[62] M. LoVerde and N. Afshordi, Phys. Rev. D **78**, 123506 (2008) [arXiv:0809.5112].